PCCP

Delayed vibrational modulation of the solvated GFP chromophore into a conical intersection

Journal:	*Physical Chemistry Chemical Physics*
Manuscript ID	CP-ART-02-2019-001077.R1
Article Type:	Paper
Date Submitted by the Author:	16-Apr-2019
Complete List of Authors:	Taylor, Miles; Oregon State University, Department of Chemistry Zhu, Liangdong; Oregon State University, Department of Chemistry; Oregon State University, Department of Physics Rozanov, Nikita; Oregon State University, Department of Chemistry; Oregon State University, School of Chemical, Biological and Environmental Engineering Stout, Kenneth; Oregon State University, Department of Chemistry; Oregon State University, School of Chemical, Biological and Environmental Engineering; Princeton University, Department of Chemistry Chen, Cheng; Oregon State University, Department of Chemistry Fang, Chong; Oregon State University, Department of Chemistry; Oregon State University, Department of Physics

Journal Name

ARTICLE

Delayed vibrational modulation of the solvated GFP chromophore into a conical intersection

Miles A. Taylor,[ae] Liangdong Zhu,[abe] Nikita D. Rozanov,[ac] Kenneth T. Stout,[acd] Cheng Chen,[a] and Chong Fang*[ab]

Received 00th January 20xx,
Accepted 00th January 20xx

DOI: 10.1039/x0xx00000x

www.rsc.org/

Green fluorescent protein (GFP) has revolutionized bioimaging and life sciences. Its successes have inspired modification of the chromophore structure and environment to tune emission properties, but outside the protein cage, the chromophore is essentially non-fluorescent. In this study, we employ the tunable femtosecond stimulated Raman spectroscopy (FSRS) and transient absorption (TA) to map the energy dissipation pathways of GFP model chromophore (HBDI) in basic aqueous solution. Strategic tuning of the Raman pump to 550 nm exploits the stimulated emission band to enhance excited state vibrational motions as HBDI navigates the non-equilibrium potential energy landscape to pass through a conical intersection. The time-resolved FSRS uncovers prominent anharmonic couplings between a global out-of-plane bending mode of ~227 cm^{-1} and two modes at ~866 and 1572 cm^{-1} before HBDI reaches the twisted intramolecular charge transfer (TICT) state on the ~3 ps time scale. Remarkably, the wavelet transform analysis reveals a ~500 fs delayed onset of the coupling peaks, in correlation with the emergence of an intermediate charge-separated state en route to the TICT state. This mechanism is corroborated by the altered coupling matrix for the HBDI Raman modes in the 50% (v/v) water-glycerol mixture, and a notable lengthening of the picosecond time constant. The real-time molecular "movie" of the general rotor-like HBDI isomerization reaction following photoexcitation represents a significant advance in comprehending the photochemical reaction pathways of the solvated GFP chromophore, therefore providing a crucial foundation to enable rational design of diverse nanomachines from efficient molecular rotors to bright fluorescent probes.

Introduction

The green fluorescent protein (GFP) from the jellyfish *Aequorea victoria* has become one of the most iconic biomolecules discovered to date. Since the extraction, purification, and characterization of GFP in the 1960s,[1,2] it has revolutionized biological and life sciences which culminated in the 2008 Nobel Prize in Chemistry.[1-6] The protein consists of a unique β-barrel structure with 238 amino acids, wherein three of them constitute the embedded chromophore. The most highly utilized property of GFP arises from its ability to be genetically encoded in living organisms (e.g., bacteria, plants, and animals) and expressed in tandem with other biomolecules. In consequence, it becomes feasible to identify and measure different parts of the cell *in vivo,* enabling the non-invasive tracking and understanding of previously unknown processes.[6,7] Recent bioimaging advances using GFP and its derivatives include stimulated emission depletion (STED), photoactivated localization microscopy (PALM), and stochastic optical reconstruction microscopy (STORM) which led to the 2014 Nobel Prize in Chemistry.[8-12]

The powerhouse within the GFP matrix is the 4-hydroxybenzylidene-1,2-dimethylimidazolinone (*p*-HBDI) chromophore (Fig. 1) that is covalently connected to the protein backbone. Inside GFP, three auto-catalyzed residues (Ser65, Tyr66, Gly67) form the chromophore, and much of the photochemistry occurs across the π-conjugated structure involving the phenol and imidazolinone rings.[13-17] When exposed to ultraviolet (UV) light, the neutral chromophore (λ_{max} = 398 nm) gains more acidity at the phenolic hydroxyl end. Excited state proton transfer (ESPT) to a nearby conserved water molecule occurs on a picosecond time scale and the resultant deprotonated intermediate I* continues to relax, ultimately emitting green light at 509 nm.[17,18] This process is highly efficient in the protein with a fluorescence quantum yield (FQY) Φ≈0.8. However, when outside of the protein matrix, Φ

[a] Department of Chemistry, Oregon State University, 153 Gilbert Hall, Corvallis, Oregon 97331-4003, USA. *E-mail: Chong.Fang@oregonstate.edu (C.F.); Fax: +1 541 737 2062; Tel: +1 541 737 6704; Web: https://fanglab.oregonstate.edu/.
[b] Department of Physics, Oregon State University, 301 Weniger Hall, Corvallis, Oregon 97331-6507, USA.
[c] School of Chemical, Biological and Environmental Engineering, Oregon State University, 116 Johnson Hall, Corvallis, Oregon 97331-8618, USA.
[d] Current address: Department of Chemistry, Princeton University, Princeton, NJ 08544, USA.
[e] M.A.T. and L.Z. contributed equally to this work.

†Electronic Supplementary Information (ESI) available: Additional discussions of the motivation and vibrational mode assignment, ESI Fig. S1–S9 on the steady-state electronic spectra of anionic HBDI in aqueous solution, ground state FSRS and Raman mode assignment, transient absorption and probe-dependent dynamics, global analysis and time constants, semi-automatic FSRS baselines, early-time dynamics of the 866 cm^{-1} marker band, FSRS spectra at late time delay points, coherent residual plot for 2D-FSRS with the control sample in 50% (v/v) glycerol-water solution, ESI Table S1–S3 on the transient absorption dynamics, excited state Raman peak intensity dynamics, and frequency shift trend of Raman marker bands *versus* the anionic HBDI chromophore ring twisting angles, and ESI references. See DOI: 10.1039/x0xx00000x

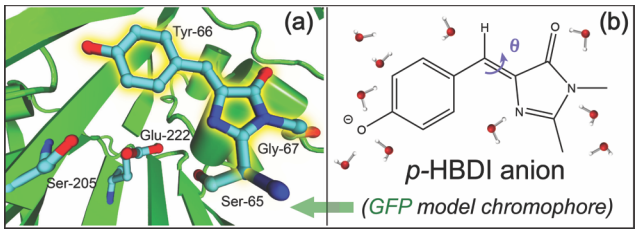

Fig. 1 A photosensitive chromophore in the local environment. (a) The chromophore highlighted in the GFP protein matrix. (b) The model GFP chromophore HBDI in its deprotonated form, surrounded by water molecules in a H-bonding network. A bridge twisting angle is depicted.

drops to ~$2x10^{-4}$ indicating that the chromophore is essentially non-fluorescent.[19,20] Prior research showed that without the intricate H-bonding network to lock the chromophore in the *cis* conformation (Fig. 1b), it undergoes photoinduced nonradiative pathways.[13,21-23]

Like other molecular rotors with aromatic rings connected by flexible chemical bonds, HBDI proceeds through a nonadiabatic conical intersection (CI) back to the electronic ground state via *cis-trans* isomerization.[19,24-26] Here we focus on the deprotonated chromophore in basic aqueous solution to avoid the competition between ESPT and ring twisting,[20,27] also because the anionic form is the green fluorescent species in GFP. The phenolate ring and adjacent imidazolinone ring represent a prime electron donor-acceptor system within one integrated molecular framework that is highly relevant to study the fleeting CIs.[17,28,29] On the picosecond timescale, HBDI undergoes a volume-conserving nuclear motion to achieve isomerization through a twisted intramolecular charge transfer (TICT) state, wherein the system accesses the CI and returns to the electronic ground state (hot to cold).[13,14,29-33] Since high-level calculations show that the CI structure with lower energy involves twisting about the bridge bond adjacent to the imidazolinone ring instead of the "hula-twist",[34,35] we depict the twisting angle θ in Fig. 1b. The exocyclic bridge C–H bond plays an important role in this photoinduced transition and should be a sensitive probe to the isomerization reaction. In this work, we implement the powerful wavelength-tunable femtosecond stimulated Raman spectroscopy (FSRS) to track an array of vibrational motions of the photoexcited anionic HBDI from ca. 300—1900 cm^{-1} and reveal key atomic motions, in a correlated manner, promoting ultrafast isomerization through a TICT state and the S_1/S_0 CI of a molecular rotor in aqueous solution. In particular, 2D-FSRS methodology has the potential to delineate the anharmonic vibrational coupling in the electronic excited state.[17,36-38] Vibrational quantum beating is of great interest due to its high sensitivity to the photoexcitation energy relaxation pathways through an intricate network of interactions between different parts or modes of the chromophore.

Results and discussion

Steady-state electronic and Raman spectra

The UV/visible absorption and spontaneous emission spectra of anionic HBDI are shown in Fig. S1 (see the ESI†). Upon 400 nm excitation of main absorption band (peak at ~425 nm), a weak emission peak is present at ~505 nm. The ground state Raman spectrum of anionic HBDI in aqueous solution (pH=10, see Fig. S2 in the ESI† with mode assignment)[39,40] shows clear peaks due to pre-resonance enhancement by the 550 nm Raman pump on the red side.[27,41] The overall peak pattern is comparable to that of the chromophore in a protein matrix (Fig. 1a), though various interactions including H-bonds inside the rigid GFP β-barrel better confine the conformational space and motions of the embedded chromophore.[17,39]

Transient absorption spectra

Upon 400 nm excitation, the fs-TA spectra of HBDI exhibit ground state bleaching (GSB) below 450 nm, an excited state absorption (ESA) band at ~473 nm, a stimulated emission (SE) band at ~519 nm, and a weak ESA band across the visible region at later times (Fig. S3 in the ESI†). The initial correlated SE and ESA dynamics indicate short-lived species on the hundreds of fs time scale. At 200 fs, the SE peak at ~502 nm is close to the spontaneous emission peak near 505 nm. At 400 fs, the SE band rapidly evolves and red shifts to 519 nm, which suggests a steep potential energy surface (PES) slope out of the Franck-Condon (FC) region.[31,41] Due to spectral overlap between the broad TA bands, we performed global analysis to delineate the correlation between ESA and SE dynamics and the excited state reaction coordinate (Fig. S4 in the ESI†).[14,42]

The retrieved subpicosecond (sub-ps) time constant is attributed to FC dynamics, which are largely insensitive to the addition of glycerol (see Table S1 in the ESI†).[14,31] The second 2–3 ps time constant is associated with a TICT state, but the third time constant, evident in the broad and long-lived ESA, has not been assigned in a time window beyond 10 ps. Vengris et al. performed pump-probe experiments with and without an fs, 530 nm dump pulse to assign the first two processes to a transition out of the FC region; however, coherent artifacts, overlapping electronic bands, and complex effects of the dump pulse hindered full spectral analysis.[14] The sub-ps generation and <2 ps decay of hot ground state species without a clear twisting coordinate remain an unresolved issue. Martinez and co-workers performed QM/MM calculations on a CI enhanced by a polar solvent.[43] For the GFP chromophore anions in gas phase, recent time-resolved action spectroscopy showed that by lowering the temperature to ~100 K or embedding in a protein pocket like GFP,[35] the energy barrier leading to the CI can be increased to enable fluorescence from a trapped excited state (lasting for ~1.2 ns). These findings stress the intrinsic chromophore capability to fluoresce when the energy barrier to nonradiative internal conversion is sufficiently high.

Excited state FSRS spectral dynamics

To elucidate atomic motions accompanying the photoinduced electronic redistribution and unambiguously track the structural evolution of GFP model chromophore in the excited state, tunable time-resolved FSRS was implemented. Previous experiments using an 400 nm actinic pump and 800 nm Raman pump yielded weak signals from solvated chromophores due to

the off-resonance conditions.[41,44] Sufficient signal-to-noise ratios can be achieved by tuning the Raman pump to 550 nm, located at the red side of the SE band that dominates the early-time transient absorption spectra of the chromophore (Fig. S3, ESI†).[27,41] This strategy has been proven highly effective in studying the primary events of a wide range of chemical and biological systems.[38]

Following 400 nm photoexcitation, the anionic HBDI chromophore in the first singlet excited state (S_1) starts to dissipate energy, tracked by the Raman pump-probe pair. For the pre-resonantly enhanced Raman modes, semi-automatic baselines were drawn (Fig. S5, ESI†) and subtracted from the spectra. The resultant time-resolved Raman spectra (Fig. 2) reveal an array of excited state modes that promptly emerge at time zero and largely disappear after a few ps. The phenolate ring hydrogen out-of-plane (HOOP) motion with bridge HOOP motion at 866 cm^{-1} and the imidazolinone ring C=N, C=O and bridge C=C stretching motion at 1572 cm^{-1} are assigned on the basis of TD-DFT calculations (see Table S2 in the ESI†), and their activity in S_1 can be closely associated with the photoinduced isomerization pathway of the solvated HBDI. Their excited state nature is corroborated by the prompt frequency shift from S_0 peak positions around photoexcitation time zero,[17,45] e.g., 1241→1253 cm^{-1}, 1558→1572 cm^{-1} in Fig. 2a, and their continuous frequency shift in S_1 on the few picosecond time scale (see Table 1) which tracks characteristic atomic motions.

Besides Raman intensity decay that typically reflects the loss of excited state population, the peak center frequency shifts track the molecular structure evolution more directly (i.e., with no competing factors like resonance conditions or electric polarizabilities that could affect the observed Raman mode intensity).[38] In essence, vibrational frequency shifts in FSRS are telltale signs that molecular structural changes occur. In Fig. 2a, the ~866 and 1253 cm^{-1} marker bands blue shift while the 1572 cm^{-1} marker band exhibits an initial blue shift before a subsequent red shift on the fs to ps time scales (Table 1), reaching a spectral silent region after ~6 ps.

To gain deeper structural insights into these characteristic vibrational frequency dynamics, the DFT calculations were performed on HBDI as a function of the θ dihedral angle[24,31,46,47] (see Experimental Methods below and Fig. 1b, around the exocyclic C=C bond) to uncover any apparent frequency shifts of these key modes (Table S3 in the ESI†). Specifically, when twisted with a positive θ angle and the imidazolinone carbonyl swings out of the plane of the phenolate ring, the calculation results largely match the observed marker band frequency shifts in solution (Fig. 2, Table 1). We note that the 866 cm^{-1} mode in both S_0 and S_1 mostly concentrates on one side of the chromophore framework (Table S2 in the ESI†).

The Raman peak intensity dynamics in S_1 are generally fit with a biphasic decay, wherein a prominent sub-ps decay is followed by a few ps component.[48,49] The first time constant is largely unaffected by the presence of glycerol and attributed to FC dynamics, likely involving local solvent motions that rapidly accommodate the wiggling chromophore.[48,50] The 2–3 ps time constant is corroborated by a frequency shift of the Raman modes and likely corresponds to a conformational change leading to the TICT state, while further relaxation within that

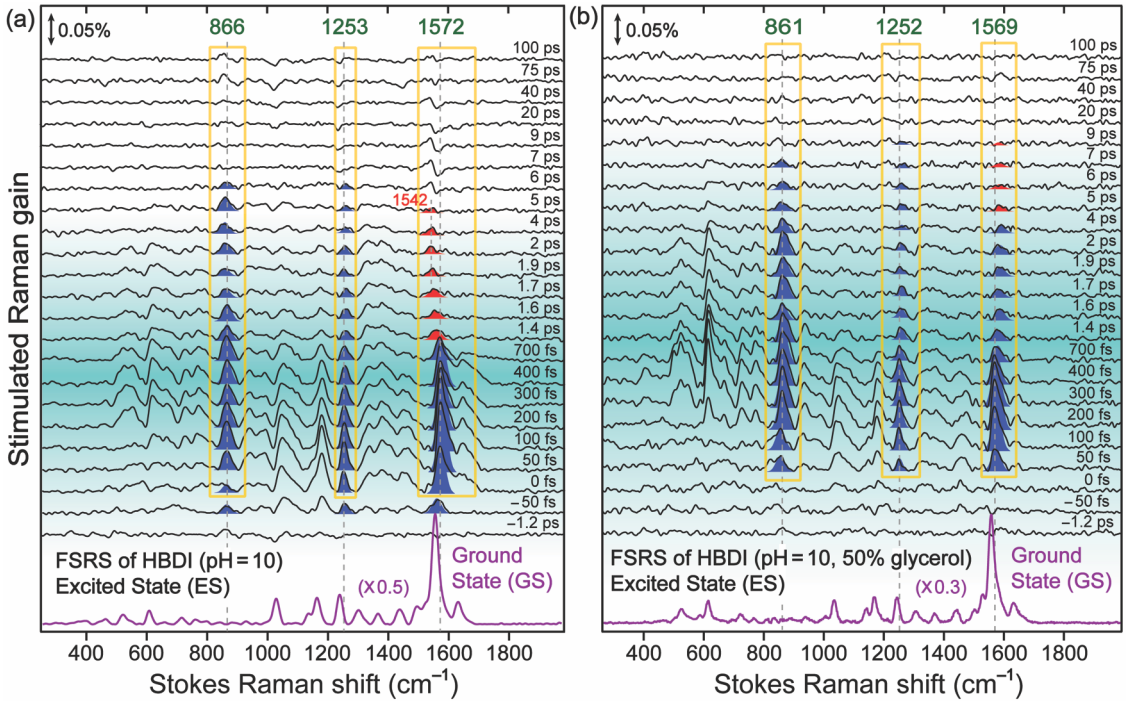

Fig. 2 Excited state FSRS data of HBDI in pH=10 aqueous solution (a) without and (b) with 50% (v/v) glycerol at representative time delay points following 400 nm photoexcitation. Transient Raman marker bands are denoted by Gaussian profiles with rise and decay on the fs to ps time scales. The semi-transparent cyan shades highlight the vibrational intensity decay into a CI. The ground-state bleach is insignificant at early times due to the resonance conditions favoring excited state peaks. The scaled ground state spectra (violet) are plotted below the ground-state-subtracted excited state spectra (black) for comparison.

state takes much less time to reach the CI.[51] Our important finding via the time-resolved excited-state FSRS is that several Raman modes, especially the 866 cm^{-1} mode (see Fig. 2a), exhibit pronounced intensity oscillations within the first ~2 ps (Fig. S6, ESI†). After subtracting the biphasic decay component, Fourier transform analysis yields two modulation modes at ~45 cm^{-1} (minor) and 230 cm^{-1} (major). Global analysis of the time-resolved FSRS data[26,52] can then generate the 2D-FSRS plot to directly visualize the anharmonic coupling map across active vibrational modes in the electronic excited state,[17,37,38] which is a powerful line of inquiry and will be further discussed below.

The subsequent question about structural snapshots is the assignment of late-time features that could imply a hot ground state. Many of the modes in Fig. 2 reappear past ~6 ps but they are mixed with the ground state bleaching. Therefore, spectral addback was conducted for better clarification (Fig. S7, ESI†). These late-time peaks at ~1545 cm^{-1} are shifted by 13 cm^{-1} from the original S_0 peak and 27 cm^{-1} from the early-time S_1 peak, but they are similar in frequency to the later-time S_1 peak at ~1542 cm^{-1} (see Fig. 2a). This observation indicates that after ~6 ps, notable spectral changes are due to a transition between electronic states, likely through a twist around the bridge C=C bond.[19,31,53] In other words, the arrival at the TICT state on the few picosecond time scale results in a Raman mode frequency red shift (1572→1542 cm^{-1}), while the CI located at the bottom of the TICT state should efficiently bring the chromophore back to the ground state with a still twisted conformation (e.g., *trans* isomer that exhibits a weakened double bond).[39,40] This non-equilibrium ground state relaxes with a ~200 ps time constant (Fig. S4, ESI†). With different resonance Raman conditions for these transient species back in S_0, we observed dispersive Raman peak line shapes at late time points in Fig. 2 because the "cold" ground state depletion peak overlaps with the "hot" ground state absorption peak mainly on the redder side.[38,54] They gradually diminish on the hundreds of ps time scale while the original ground state is recovered to a greater extent.[53]

Table 1 Frequency dynamics of the excited state marker bands of anionic HBDI in water

With 0% Glycerol		With 50% Glycerol	
Raman mode (cm^{-1})	Frequency blue shift time constants [a]	Raman mode (cm^{-1})	Frequency blue shift time constants [a]
866	340 ± 80 fs 2.1 ± 0.1 ps	861	350 ± 100 fs 3.0 ± 0.1 ps
1253	270 ± 30 fs 2.2 ± 0.1 ps	1252	275 ± 75 fs 3.0 ± 0.1 ps
1572	330 ± 25 fs 2.1 ±0.1 ps [b]	1569	375 ± 50 fs 3.1 ± 0.1 ps [b]

[a] The uncertainties are shown as one standard deviation (±1 s.d.) of the time constants from least-squares fits of the experimental data sets (N=3) in water at room temperature. [b] These picosecond time constants are associated with the specific vibrational mode frequency red shift as a major component.

Notably, similar time constants are retrieved from TA (see Table S1 in the ESI†) and FSRS (Table 1) data on the 200–400 fs and 2–3 ps time scales for the anionic HBDI in pH=10 aqueous solution. This close match substantiates a clear separation of transient electronic states along a photoexcited chromophore isomerization coordinate (*vide infra*),[13,19,31] with characteristic vibrational motions elucidated by the time-resolved FSRS.

Vibrational coupling from global analysis of FSRS

When the chromophore is embedded in the protein pocket, the ~1262 and 1565 cm^{-1} modes were found to be anharmonically coupled to a low-frequency mode that facilitates the ESPT reaction.[17,55] In the pH=10 aqueous solution, the anionic HBDI has no dissociable proton so it undergoes other excited state relaxation processes. Our experiments in this work afford the opportunity to (1) reveal the existence of functional low-frequency modes in a simpler microenvironment than a protein, and (2) compare the underlying mechanism for ESPT[17,38] and ring twisting on a dynamic PES. To retrieve quantum beating reliably across the entire detection window, we performed global analysis using Glotaran on the FSRS spectra in Fig. 2. With a three-component kinetic model analogous to the one used for TA analysis (Fig. S4 in the ESI†), transient spectra were fit using an iterative least-squares minimization process up to 2 ps with 50 fs time steps. The global fit was then subtracted from the raw data to obtain the coherent residuals, which exhibit multi-mode oscillations with largely in-phase patterns across various modes (Fig. S8, ESI†), particularly for the ~872 and 1571 cm^{-1} marker bands. The non-uniform oscillations imply contributions from multiple low-frequency modes. Meanwhile, the addition of 50% (v/v) glycerol in aqueous solution results in notable changes of the oscillation period, which indicates that hindrance of the chromophore two-ring twisting by the viscous glycerol affects the solute normal mode frequency, both the intramolecular and intermolecular vibrational coupling matrix, and hence the photoexcited energy relaxation pathways.

To provide a quantitative and rigorous representation of the quantum beating phenomenon, we then performed a discrete Fourier transform (FT) of the frequency-dispersed residuals along the time axis. The resultant 2D-FSRS map reveals the anharmonic vibrational coupling that facilitates energy transfer and dissipation of a photoexcited molecule in aqueous solution. Notably, a Hamming window was applied to reduce the edge artifacts and overall noise before FT analysis to achieve a frequency range of 1—330 cm^{-1} and a resolution of 1 cm^{-1}. The analysis of data in Fig. 2a and b compares all the spectral modes at once (see Fig. 3, and Fig. S9 in the ESI†), rather than selecting certain modes to apply FT (Fig. S6, which nicely validates the 2D-FSRS approach). The output power spectrum provides an estimate of the spectral density (i.e. periodogram) within 0–2 ps. Remarkably, a low-frequency mode at ~227 cm^{-1} (Fig. 4a) modulates several high-frequency modes, though to varying degrees because the pertinent skeletal motions could be divided into reactive and unreactive ones.[37] In the Raman marker band assignment (Table S2 in the ESI†) we note that all the coupling modes in Fig. 3 involve the exocyclic bridge region

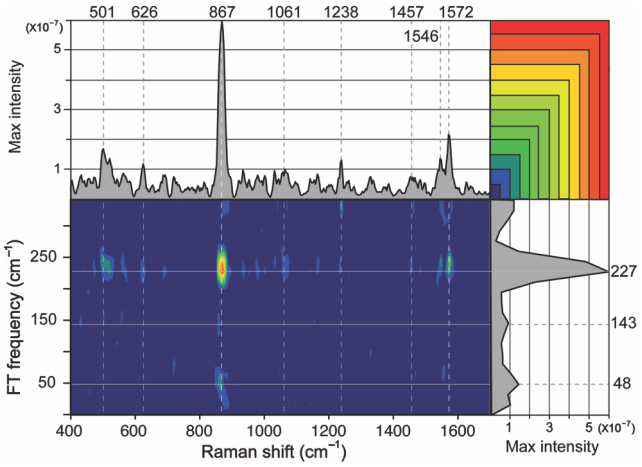

Fig. 3 2D-FSRS of the HBDI anion in aqueous solution infers prominent vibrational coupling between Raman marker bands up to 2 ps after 400 nm photoexcitation. The maximal values projected onto the Raman shift axis and FT frequency axis are shown as the 1D plot above and to the right side of 2D-FSRS plot, respectively. The dashed lines highlight those prominent coupling peaks, and the pertinent chromophore vibrational mode assignments are listed in Table S2 in the ESI†.

(C or H atoms, Fig. 1b). In comparison to the impulsively excited ~120 cm^{-1} mode revealed in the wild-type GFP that gates ESPT reaction,[17] the HBDI anion in solution also manifests one dominant vibrational coordinate along the photophysical as well as photochemical reaction coordinate. Remarkably, a different motion (227 cm^{-1}) is now uncovered in an altered environment. The interesting and important question arises: does this low-frequency mode accompany or facilitate the chromophore isomerization in aqueous solution?

Since the 227 cm^{-1} mode is attributed to a global ring OOP deformation and bridge C–C–C OOP bending motion of the chromophore (Table S2 in the ESI†) as depicted in Fig. 4a, it could be coupled to the 866 cm^{-1} mode as shown in Fig. 4b via through-bond interactions.[56] The OOP nature of these modes modulating and being modulated is intimately related to the aqueous environment, sensing less steric hindrance than that in a protein matrix. As a result, the active 227 cm^{-1} delocalized mode close to FC region could couple to a more localized ~866 cm^{-1} mode toward the TICT state, but the detailed mechanism and relevant time scale for such a functional correlation require further experimental data analysis (see discussions below). To a lesser extent, vibrational coupling also occurs between the 227 cm^{-1} OOP mode and an in-plane mode at ~1572 cm^{-1} (Fig. 4c) which are both global motions over the two-ring system. This result substantiates the prominent activity of the 227 cm^{-1} mode modulating several vibrational motions within ~2 ps after photoexcitation, and the multidimensional nature of the PES leading to conformational twisting (see supporting text in the ESI†). In order to swiftly reach the CI without undergoing any significant radiative transition back to S_0, the photoexcited molecule needs to efficiently explore the phase space via coupling a global OOP mode to a number of selective OOP and in-plane modes, which correspond to the few prominent peaks observed in the 2D-FSRS map (Fig. 3 and Fig. S9, ESI†).[37,57]

Wavelet transform of the coherent oscillations unveils a transient electronic state

To understand the intrinsic frequency dynamics of coherent residuals after global analysis of the time-resolved FSRS data, we apply the continuous wavelet transform (CWT) to a 1 cm^{-1} slice along the residuals at 866 cm^{-1} using a Morlet wavelet with a 2π central frequency.[58,59] The resultant information about localization of certain modes through time is critical to dissect the photoinduced reaction coordinate frame by frame. Notably, the CWT spectrum retains the same characteristic features over a broad range of wavelet parameters (e.g., shifting octaves from 1–10 and voices from 2–16 with any combination), validating the results as inherent in our experimental data. Two octaves and eight voices were chosen to yield a frequency range from ~1 to 330 cm^{-1} (i.e., Nyquist frequency corresponding to the experimental time step of 50 fs) and a smooth plot in Fig. 5.

For the HBDI anion in aqueous solution (data in Fig. 2a and Fig. 3), the CWT analysis (Fig. 5) reveals that the excited state 227 cm^{-1} "modulating" mode does not appear at the time zero of photoexcitation, but its peak intensity starts to rise after a short dwell of ~500 fs. Since the excited state 227 cm^{-1} mode is anharmonic and non-totally symmetric, the delayed onset of its apparent coupling to certain higher frequency modes (e.g., 866

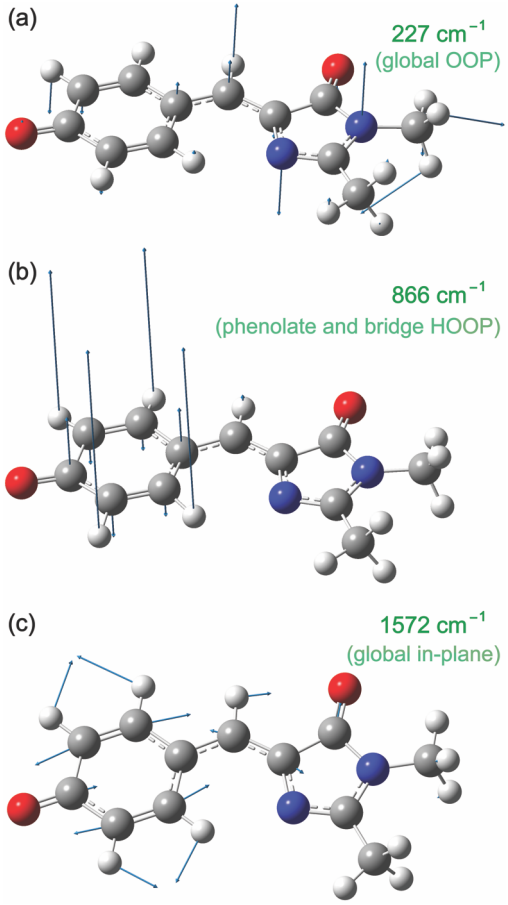

Fig. 4 Characteristic atomic motions based on the TD-DFT normal mode calculations of HBDI anion in aqueous solution. The (a) 227, (b) 866, and (c) 1572 cm^{-1} modes are depicted in ball-and-stick models with C, N, O, H atoms in gray, blue, red, and white spheres, respectively.

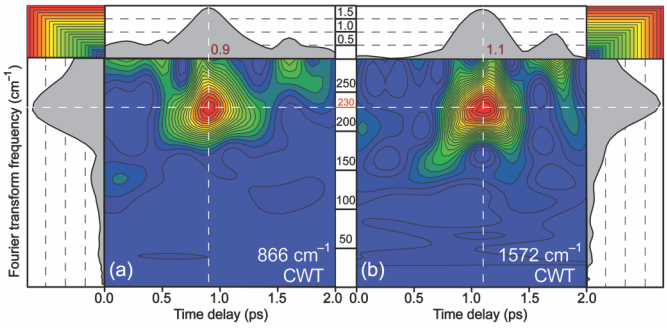

Fig. 5 Continuous wavelet transform (CWT) of the anionic HBDI Raman bands with the pronounced intensity oscillations following 400 nm photoexcitation. For the (a) 866 and (b) 1572 cm^{-1} modes, the time-frequency map after CWT of coherent oscillations manifests a dominant modulating mode. The projection of maximal values onto two axes is shown separately in gray shades. The white dashed lines highlight the peak frequency at ~230 cm^{-1} and a delayed peak maximum at ~1 ps.

and 1572 cm^{-1}) indicates that (1) the intrinsic off-diagonal element in the molecular Hamiltonian is not the sole determinant for the observed quantum beats, and (2) there could be ultrafast energy flow between the FC modes and reactive modes across a broad spectral region especially when an fs excitation pulse is used. In other words, the impulsively generated coherent vibrational motions in the FC region could transfer energy to the 227 cm^{-1} mode on the sub-ps time scale and lead to coherent motions of those energy-accepting modes. This type of underdamped torsional motion with intramolecular vibrational redistribution (IVR) in a polar medium has been shown to play important roles in a great variety of photochemical reactions.[17,32,48,60-62] Corroborating evidences from the fs-TA results include the delayed appearance of the maximal SE magnitude at ~400 fs (Fig. S3c in the ESI†), and the transient ESA rise time constant of ~350 fs (Fig. S3d in the ESI†) that matches the SE decay time constant of ~400 fs (Table S1 in the ESI†). These spectral data infer an intermediate S_1 state of the anionic HBDI chromophore with charge-separated (CS, not a complete electron transfer) character that is typical for photoacidic molecules,[42,63,64] particularly for the anionic species in S_1 with a reduced dipole as it is less solvated than in S_0.[47,65-67]

Our key finding is therefore the correlation between this CS state and the onset of quantum beating (Fig. 5), which can be further rationalized. First, the time constant for the CS state formation (~350 fs) matches the initial sub-ps decay of S_1 Raman modes (Table S2 in the ESI†), and the rise of the CWT peak (Fig. 5). Second, the coupling between a global 227 cm^{-1} OOP deformation mode and a more localized 866 cm^{-1} phenolic ring and bridge HOOP mode suggests an intricate sequence of ultrafast charge transfer (from the phenolate oxygen site toward the imidazolinone ring) and collective atomic motions (concentrated on the phenolate ring up to ~2 ps). Third, two temporal components of the S_1 Raman mode dynamics exhibit different dependence on solvent viscosity wherein the sub-ps time constant is less sensitive to the addition of 50% glycerol (Table S2 in the ESI†). The CS state formation due to charge redistribution over the chromophore two-ring system occurs on this sub-ps time scale,[42,68] enabling the 227 cm^{-1} mode to effectively modulate the 866 and 1572 cm^{-1} modes (Fig. 5) for ~1 ps duration and guide the system into the TICT state.[28,29,37] This reaction coordinate is supported by the lengthened second time constant of the S_1 Raman mode on the ps time scale when 50% (v/v) glycerol is added to increase the solvent viscosity and hinder chromophore twisting. The essence of this nonadiabatic vibrational coupling can be compared to a recent 2D electronic spectroscopic study on artificial systems with controllable energy gaps and resonantly enhanced vibronic coupling,[69] which substantiates the importance of structural rigidity and system-bath interaction in determining the pathways and efficiency of photoexcitation energy dissipation and transfer.

Functional roles of conformational motions after the FC region

The observed vibrational modulations of OOP skeletal motions in FSRS provide compelling new knowledge for the conformational twisting pathway as HBDI proceeds into a TICT state. The S_1 Raman modes promptly emerge around the time zero of photoexcitation (Fig. 2), shifted from the corresponding S_0 modes, which confirms their excited state nature. The high signal-to-noise ratios of the chromophore modes benefit from the increased electric polarizability in S_1 and the favorable resonance enhancement effect by the 550 nm Raman pump. However, these S_1 Raman bands are likely spectators modes along the reaction coordinate on the excited state PES[17,30,44,60] unless there is clear spectral evidence that infers the directional energy transfer between certain vibrational motions to surmount the symmetry barrier between the excited and ground states.[28,37] The search for functional nuclear motions leads us to sequentially perform the (1) global analysis of the entire time-resolved FSRS data sets, (2) 2D-FSRS analysis by FT, and (3) time-frequency analysis of the dominant modulating/tuning modes by CWT.

The most striking result is the delayed onset of intensity oscillations of two transient Raman marker bands, separated by >700 cm^{-1}, while the temporal dwell of ~500 fs matches an intermediate electronic state formation time. Once in the CS state, the bond order in the ethylenic bridge changes (Fig. 1b) as the electrons migrate from the phenolate CO^- to the imidazolinone ring (i.e., intramolecular charge transfer), thus providing an avenue for the 227 cm^{-1} mode to modulate an OOP mode localized on the phenolate ring and to a lesser extent, an in-plane stretching mode concentrated on the imidazolinone ring. Since the CS state decay time constant lengthens upon adding 50% glycerol (see Table S1 in the ESI†, the second time constant), the delayed chromophore ring twisting motions are likely involved that lead to the formation of a TICT state which lies lower than the CS state in the excited state PES (see Fig. 6). The pertinent structural change is echoed by the excited state vibrational frequency shifts of the 866, 1253 and 1570 cm^{-1} modes (Figure 2 and Table 1).

Inspired by a former study that showed a bimolecular π-stacked CT complex using anharmonic vibrational coupling to access a CI and achieve radiationless charge recombination (CR),[28] we surmise that the crossing of a small energy barrier between the CS and TICT state (Fig. 6) is facilitated by the

aforementioned anharmonic vibrational coupling. The newly "activated" global OOP motion probably needs to settle more into concentrated motions on the phenolate and imidazolinone rings separately so the loss of two-ring chromophore coplanarity would be permitted at a reduced energy cost. This rationale is reminiscent of the 2D dynamics involving a slow and fast mode in S_1,[31] which could be associated with the 866/1572 and 227 cm^{-1} mode (see Fig. 2 and 4), respectively. Though the TICT state could be considered to have a peaked CI that permits rapid nonadiabatic transition into S_0 which bifurcates into the *cis* (main) and *trans* or *trans-like* (minor) conformers,[43,70] the arrival at the TICT state is not barrierless and requires a small activation energy (hence the few ps time constant, see Table 1 and Fig. 6). This S_1/S_0 CI passage is reminiscent of the ultrafast *cis-trans* isomerization of a model protonated Schiff base in water that, as a fast solvent, supports a peaked CI topology.[71] Moreover, substantial nuclear motions of the chromophore occur before and after the CI passage that goes beyond CT and CR processes (i.e., electronic motions), characteristic of typical photoisomerization reaction without chemical bond breaking or formation.[70,72,73]

In addition, previous computations showed that the excited state *cis-trans* isomerization of HBDI is gated by protonation, and the S_1 PES of the anionic form has the smallest energy barrier (<2 kcal/mol) from the planar conformation to the twisted state and the CI point among the neutral, cationic, zwitterionic, and anionic forms in gas phase,[34] within a factor of 2 of the energy barrier calculated from transition state theory and experimental data.[35] Using the value of 8.4 kJ/mol as the upper limit of activation energy E_a (considered to be similar in solution phase as the measured rate constants showed)[74] and a barrierless reaction rate constant as the frequency factor $A \approx (k_B T/h) \approx 6.1\times10^{12}$ s^{-1} at room temperature ($T \approx 295$ K), we can use the Arrhenius equation $k = A \cdot exp(-E_a/RT)$ and estimate the excited state chromophore twisting rate constant $k \approx 2.0\times10^{11}$ s^{-1} which corresponds to a time constant of ~5 ps, largely matching the experimentally observed CS→TICT state transition time of 2–3 ps in Fig. 6. A 20% reduction of E_a to 6.7 kJ/mol yields a reaction time constant of 2.5 ps and an excellent match to the experimental value. Therefore, it is reasonable to consider that the S_1 PES governs the "facile" excited state structural dynamics of the anionic HBDI, further supported by the snapshot-based computations[34] and the photoinduced atomic motions in time-resolved FSRS (Fig. 2).

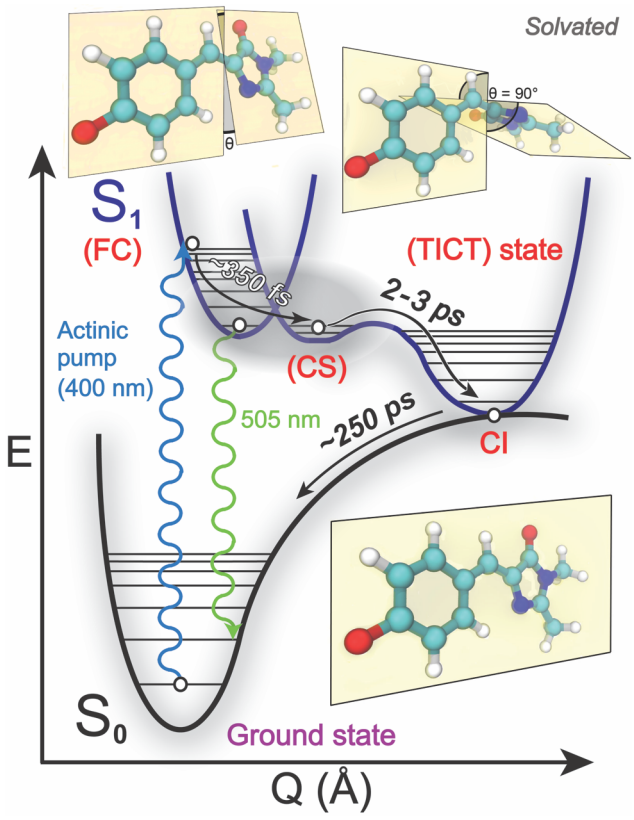

Fig. 6 Schematic PES for anionic HBDI in aqueous solution. The absorption and stimulated emission are denoted by vertical wavy lines. The energy relaxation pathways are shown by black curved arrows with time constants on ultrafast time scales. The chromophore molecular conformation with the twisting angle θ is depicted alongside the respective electronic state.

Notably, without steric constraints and a unique H-bonding network inside the GFP protein pocket, distinctive OOP skeletal motions emerge to play a commanding role in the HBDI excited state PES, responsible for the drastically reduced FQY in solution. Because the anionic HBDI has no proton to transfer, ESPT cannot play a role and alternative energy relaxation pathways need to be involved.[20] Interestingly, Chattoraj et al. used the time-resolved fluorescence spectroscopy to study the anionic chromophore of GFP after 478 nm excitation, in pH=6.5 aqueous phosphate buffer solution with 50% (v/v) glycerol, and a ~1.9 ps rise time constant was observed for the 508 nm emission peak.[18] This finding suggests that an initial vibrational and energy relaxation on the few ps time scale, likely involving charge redistribution and some volume-conserving structural motions, is a conserved property for the anionic HBDI or HBDI-like chromophoric moiety in various environments. Additional experimental support for our observed time constants comes from a previous time-resolved photoelectron spectroscopic study on the deprotonated *p*-HBDI in gas phase: the time constants of 330 fs and 1.4 ps were attributed to rotation around the bridge C–C–C bond and internal conversion back to the anion ground state,[74] remarkably similar to the chromophore relaxation in solution phase. Lastly, both the 227 and 866 cm^{-1} modes in Fig. 4 consist of little to no carbonyl motions on the imidazolinone ring, which suggests that the H-bonding to that specific atomic site remains largely intact for these vibrational motions, which may contribute to the fluorescence quenching pathway more effectively than other atomic sites on the conjugated ring system.[75]

Chromophore local environment dictates the excited state PES

Systematically investigating the chromophore structural dynamics under different conditions affords deeper insights into the interplay between local environment and fluorescence. In the protein β-barrel, steric hindrance and H-bonding to Ser205, His148, Thr203 on the phenolic hydroxyl side and Glu94, Arg96 on the imidazolinone carbonyl side (Fig. 1a) have

been shown to affect the excited state lifetime and FQY of the chromophore.[46,76,77] Such a structure-constraining effect can be rationalized by exposing the free HBDI anion to an increasing glycerol concentration, which changes the excited state dynamics and vibrational coupling. With three hydroxyl groups, glycerol introduces a different intermolecular H-bonding network to HBDI, lowering ground state energy and raising the activation energy barrier for the excited state processes.[46] Besides the longer time constants on the 2–3 ps time scale observed with 50% (v/v) glycerol (see Table 1, Table S2 in the ESI†, Fig. 6), the coherent residuals map in Fig. S8b and 2D-FSRS map in Fig. S9 significantly differ from the photoexcited HBDI in aqueous solution without glycerol (Fig. S8a and Fig. 3). This trend is in accord with the reduced 2D-FSRS peak intensity of the OOP oscillation at ~212 cm^{-1} in the water-glycerol mixture (Fig. S9), which represents a frequency red shift from the 227 cm^{-1} mode (Fig. 4a) due to a bulkier H-bonding partner to the chromophore and the increased solvent viscosity. Notably, this strong OOP mode diminishes while a ~130 cm^{-1} weak OOP mode and a 276 cm^{-1} in-plane deformation motion involving mostly the phenolate ring gain intensity in the water-glycerol mixture. Importantly, the 2D-FSRS analysis allows a clear assessment of initial structural motions of the chromophore with more steric hindrance (higher viscosity), altered electrostatics,[78] and a reduced number of H-bonds from pure water to the water-glycerol mixture. This trend is consistent with an increased FQY of HBDI in the presence of glycerol due to a raised torsional energy barrier to nonradiative internal conversion (see Fig. 6, between the CS and TICT states) or upon the chromophore conformational locking.[42,79,80]

Furthermore, our new knowledge about structural dynamics of the GFP chromophore in aqueous solution validates a previous computational study on the dominance of electrostatics over sterics in keeping the chromophore planar and producing high yield fluorescence.[78] The arrival at a distinct CS electronic state on the sub-ps time scale precedes the observed vibrational quantum beats due to the anharmonic coupling between certain vibrational modes (i.e., nuclear motions), which in turn leads to a crossing of the CI connecting two electronic states (S_1 and S_0 in this case). Besides contributions from both electron and nuclear motions, the sequence of structural events revealed by the time-resolved FSRS starting from the FC region (Fig. 2) enables us to capture the peculiar temporal dwell, a preparation stage *per se* (Fig. 5), that substantiates the importance of intrinsic electronic structure of GFP chromophore. The resultant multidimensional PES as depicted in Fig. 6 is the very reason we observed via 2D-FSRS a delayed onset of the coherent mode at 227 cm^{-1} modulating the ~866 and 1572 cm^{-1} modes (Fig. 3), and the significance of a global OOP motion that emerges with the photoinduced charge separation during FC relaxation and then facilitates the subsequent formation of a TICT state.

More generally, for photochemical reactions that occur on the time scale of <10 ps, vibrational coherences likely play a significant role regardless in gas or condensed phase.[17,37,57,68] The highly displaced, impulsively excited low-frequency modes by the fs photoexcitation pulse lead to efficient wavepacket spreading on the PES, which could involve higher vibrational states as well, but the HBDI chromophore conjugated two-ring torsional barrier is non-negligible (Fig. 6). Meanwhile, previous fluorescence line shape analysis on the anionic HBDI versus wtGFP at various temperatures suggested strong vibronic coupling of the fluorescent state (the FC and CS state in Fig. 6) to the torsional deformation of the chromophore,[51] which should involve a range of nuclear coordinates instead of a single, isolated point at the CI.[31] In this work, the "coordinated" motions via anharmonic coupling are observed prior to internal conversion through the S_1–S_0 conical intersection, which provide previously hidden information about the onset of functional torsional motions and their effect on the coupled multiple vibrational modes. Due to solute-solvent interactions and the resultant change to the PES guiding the excited state energy dissipation pathways, the control experiment by adding 50% (v/v) glycerol to the aqueous solution further corroborates the robustness of the CWT analysis based on the semi-automatically generated 2D-FSRS map, and the new structural dynamics insights into the photoinduced isomerization reaction of the solvated GFP chromophore.

Experimental methods

Synthesis and sample preparation

HBDI was synthesized in a two-step reaction from 4-hydroxybenzaldehyde and iminoglycine methyl ester following previous procedures and used without further purification.[81] The ^{1}H NMR spectrum of the product was checked to be consistent with previous reports.[39,82] Aqueous solutions of ~1 mM HBDI at pH=10 (with 1 mM K_2CO_3) were prepared with the additional glycerol concentrations of 0% and 50% (v/v).

Steady-state electronic spectroscopy

The absorption and emission spectra of HBDI solutions were measured by the Evolution 201 UV/Visible (Thermo Scientific) and F-2500 fluorescence (Hitachi) spectrophotometers, respectively, at room temperature. The UV/Visible spectra of anionic HBDI in aqueous solution were collected before and after each FSRS experiment, and a typical 10–12% decrease of the main 425 nm absorption peak intensity was observed due to some photoinduced irreversible change of the sample[17,41] or it may take longer time after 400 nm laser irradiation to fully recover the original sample thermally equilibrated state via a ground-state isomerization reaction.[83]

Transient absorption spectroscopy

Our detailed setup for femtosecond transient absorption (fs-TA) has been reported.[50] In brief, a Ti:Sapphire fs oscillator (Mantis-5) seeds a regenerative laser amplifier (Legend Elite-USP-1K-HE, Coherent, Inc.) to generate the 4 W, 35 fs, 800 nm fundamental output with a repetition rate of 1 kHz. A portion of the fundamental beam was frequency doubled in a 0.3-mm-thick type-I BBO crystal to obtain the pump and then attenuated to ~0.5 mW. The supercontinuum white light (SCWL) probe from ca. 400—750 nm was achieved in a 2-mm-thick quartz cell filled

with deionized water. Cross-correlation time of ~150 fs was measured from optical Kerr effect in a standard solvent such as methanol. The pump and probe pulses were overlapped in a 1-mm-pathlength quartz sample cell and dispersed in a spectrograph (Oriel MS127i) onto a front-illuminated CCD array camera (PIXIS 100F, Princeton Instruments). All the spectral data acquisition was performed by a custom LabVIEW suite (National Instruments). For global analysis of fs-TA data, the Glotaran software was used.[84]

Wavelength-tunable FSRS

Details of our FSRS setup can be found elsewhere.[41,44,55,85] Three laser pulses are needed to collect the time-resolved Raman signal in the frequency domain, including an actinic pump, Raman pump, and Raman probe. Analogous to fs-TA, the actinic pump was generated via second harmonic generation of the 800 nm fundamental while the SCWL probe was generated in water. The Raman pump at 550 nm arose from a home-built two-stage ps noncollinear optical parametric amplifier (NOPA). With the power adjusted by neutral density filters, all beams were focused on the 1-mm-thick quartz cuvette using a parabolic mirror while the sample solution was constantly stirred. The stimulated Raman scattering signal emitted collinearly with the probe is dispersed in a spectrograph (Acton SpectraPro SP-2300, Princeton Instruments) onto a CCD camera and collected by the LabVIEW program. Experiments with the Raman pump at 505 or 570 nm led to dispersive or weaker signals so the 550 nm Raman pump represents an optimal wavelength case for pre-resonance enhancement that supports the detailed data analysis and interpretations (see above).[38,41]

Computational methods

Quantum calculations and normal mode analysis of HBDI were conducted using density functional theory (DFT) and time-dependent (TD)-DFT in Gaussian 09.[86] The dihedral angle of HBDI was fixed at different values (θ=0°, ±20°, ±40°, ±60°, ±80° and ±90°, see Fig. 1b and Table S3) in DFT calculations to uncover the effect on vibrational frequencies of the anionic chromophores in water. Geometry optimization and vibrational frequency calculations were performed at a RB3LYP exchange-correlation functional level[87] with a basis set of 6-31G+(d,p), using IEFPCM-water method as the implicit solvation model.[86]

FSRS data analysis

Recording the excited-state stimulated Raman spectra in the frequency domain requires baseline removal at each time delay. In this work, the FSRS data were processed both manually and semi-automatically without notable difference in the resultant peak properties and dynamics, likely benefiting from high signal-to-noise ratios (SNRs) with the resonance enhancement of transient Raman peaks of the solute molecules.[41] An asymmetric least-squares algorithm was used in the programming language R with a smoothing parameter λ = 4 and residual weighting p = 0.004, generating the baseline that was subtracted from each trace.[88] This numerical method provides a robust baseline estimate while simultaneously optimizing only two adjustable parameters. Notably, the R-generated baselines seem to be largely lower envelopes of the transient FSRS spectra (see Fig. S5 in the ESI†). This is because the experimental spectra mostly consist of the dominant positive excited-state Raman features due to favorable resonance enhancement conditions at early times (<5 ps, 520 nm the S_1 SE peak), while the ground state bleaching signal is within the SNR due to the small percentage (~10%) of sample populations being photoexcited[17,45] and the much less favorable resonance conditions (i.e., 425 nm the S_0 absorption peak with the 550 nm Raman pump).[38,54] The semi-automatic approach requires little human input and produces reasonable baselines as compared with the spline baselines manually drawn and confirmed by visual inspection.

Conclusions

Using the recently developed tunable FSRS technique with semi-automatic baseline subtraction and 2D-FSRS-based wavelet transform analysis, aided by transient absorption (TA) and density functional theory calculations, we have shed new light on the multidimensional excited state energy landscape of a GFP model chromophore in aqueous solution. Detailed correlation between the electronic population dynamics from TA and the vibrational intensity and frequency dynamics from FSRS reveals the formation of an intermediate CS state on the ~500 fs time scale, when a dominant 227 cm^{-1} out-of-plane vibrational modulation emerges to guide the chromophore into a TICT state with a 2–3 ps time constant. The anionic chromophore two-ring twisting motion via an ethylenic bridge is delineated to have a weak dependence on solvent viscosity and H-bonding pattern in aqueous solution with 0% or 50% (v/v) glycerol, albeit with a notably changed anharmonic coupling matrix with a suppression of out-of-plane modulating modes. This comparison provides strong evidence for the functional relevance of characteristic low-frequency skeletal motions in facilitating the photoexcited chromophore to cross over into the TICT state and return to the electronic ground state via a conical intersection. Within the time-resolved FSRS plot up to 100 ps after photoexcitation, the pre-resonantly enhanced excited state Raman modes decay into a spectral "silence" region on the few ps time scale (i.e., passing through a conical intersection), followed by spectral features associated with a hot ground state on the hundreds of picosecond time scale. The isomerized chromophore gradually twists back to the *cis* conformation, evidenced by a ~200 ps time constant retrieved from global analysis of TA spectra as well as the decrease of ground state addback ratio in the long-time FSRS spectra.

The uncovered 227 cm^{-1} modulating mode with a distinct temporal dwell associated with a nascent charge-separated electronic excited state is crucial in understanding the result of any excitation of the system, regardless of the coherent (e.g., fs laser pulses) or incoherent (e.g., sunlight) nature of incident light source. The dominant vibrational anharmonic coupling to the ~866 and 1572 cm^{-1} modes with a ~500 fs dwell after photoexcitation is a key finding of this work. The temporal match between the onset of anharmonic vibrational coupling

and an intermediate charge-separated state on ultrafast time scales is a prime example of correlated electronic and nuclear motions which are likely ubiquitous for efficient photochemical reactions.

Tunable FSRS allows us to elucidate "elusive" photoinduced relaxation pathways of anionic HBDI in aqueous solution, and show that the interplay between certain out-of-plane and in-plane modes likely facilitates the efficient internal conversion from a CS state via a TICT state and conical intersection to the ground state. This crucial component of the system Hamiltonian of the GFP "heart" outside its protein matrix, illuminated through 2D-FSRS and wavelet transform analysis, will guide the rational design and future advances to power many exciting molecular machines with improved or new functions.

Conflicts of interest

There are no conflicts of interest to declare.

Acknowledgements

This work was supported by the NSF CAREER grant (CHE-1455353) and OSU Research Equipment Reserve Fund (Spring 2014) to C.F. The OSU Chemistry Bruce Graham Memorial Fellowship (Summer 2018, to M.A.T.) and Wei Family Private Foundation Scholarship (2014–2019, to C.C.) for research and student support are greatly appreciated. We also thank Dr. Longteng Tang, Dr. Breland Oscar, and Taylor Krueger for helpful discussions.

Notes and references

1 O. Shimomura, F. H. Johnson and Y. Saiga, *J. Cell. Comp. Physiol.*, 1962, **59**, 223-239.
2 O. Shimomura, *FEBS Lett.*, 1979, **104**, 220-222.
3 M. Chalfie, Y. Tu, G. Euskirchen, W. W. Ward and D. C. Prasher, *Science*, 1994, **263**, 802-805.
4 R. Y. Tsien, *Annu. Rev. Biochem.*, 1998, **67**, 509-544.
5 M. Zimmer, *Chem. Soc. Rev.*, 2009, **38**, 2823-2832.
6 P. Dedecker, F. C. De Schryver and J. Hofkens, *J. Am. Chem. Soc.*, 2013, **135**, 2387-2402.
7 G. Jung, (Ed.), *Fluorescent Proteins II: Application of Fluorescent Protein Technology*, Springer-Verlag, Berlin Heidelberg, 2012.
8 S. W. Hell and J. Wichmann, *Opt. Lett.*, 1994, **19**, 780-782.
9 E. Betzig, G. H. Patterson, R. Sougrat, O. W. Lindwasser, S. Olenych, J. S. Bonifacino, M. W. Davidson, J. Lippincott-Schwartz and H. F. Hess, *Science*, 2006, **313**, 1642-1645.
10 M. J. Rust, M. Bates and X. Zhuang, *Nat. Methods*, 2006, **3**, 793-796.
11 W. E. Moerner, *Proc. Natl. Acad. Sci. U. S. A.*, 2007, **104**, 12596-12602.
12 B. Huang, H. Babcock and X. Zhuang, *Cell*, 2010, **143**, 1047-1058.
13 N. M. Webber, K. L. Litvinenko and S. R. Meech, *J. Phys. Chem. B*, 2001, **105**, 8036-8039.
14 M. Vengris, I. H. M. van Stokkum, X. He, A. F. Bell, P. J. Tonge, R. van Grondelle and D. S. Larsen, *J. Phys. Chem. A*, 2004, **108**, 4587-4598.
15 A. A. Pakhomov and V. I. Martynov, *Chem. Biol.*, 2008, **15**, 755-764.
16 K. M. Solntsev, O. Poizat, J. Dong, J. Rehault, Y. Lou, C. Burda and L. M. Tolbert, *J. Phys. Chem. B*, 2008, **112**, 2700-2711.
17 C. Fang, R. R. Frontiera, R. Tran and R. A. Mathies, *Nature*, 2009, **462**, 200-204.
18 M. Chattoraj, B. A. King, G. U. Bublitz and S. G. Boxer, *Proc. Natl. Acad. Sci. U. S. A.*, 1996, **93**, 8362-8367.
19 D. Mandal, T. Tahara and S. R. Meech, *J. Phys. Chem. B*, 2004, **108**, 1102-1108.
20 T. Chatterjee, F. Lacombat, D. Yadav, M. Mandal, P. Plaza, A. Espagne and P. K. Mandal, *J. Phys. Chem. B*, 2016, **120**, 9716-9722.
21 M. Zimmer, *Chem. Rev.*, 2002, **102**, 759-781.
22 M. E. Martin, F. Negri and M. Olivucci, *J. Am. Chem. Soc.*, 2004, **126**, 5452-5464.
23 L. M. Tolbert, A. Baldridge, J. Kowalik and K. M. Solntsev, *Acc. Chem. Res.*, 2012, **45**, 171-181.
24 W. Weber, V. Helms, J. A. McCammon and P. W. Langhoff, *Proc. Natl. Acad. Sci. U. S. A.*, 1999, **96**, 6177-6182.
25 N. Amdursky, Y. Erez and D. Huppert, *Acc. Chem. Res.*, 2012, **45**, 1548-1557.
26 C. R. Hall, J. Conyard, I. A. Heisler, G. Jones, J. Frost, W. R. Browne, B. L. Feringa and S. R. Meech, *J. Am. Chem. Soc.*, 2017, **139**, 7408-7414.
27 L. Tang, W. Liu, Y. Wang, L. Zhu, F. Han and C. Fang, *J. Phys. Chem. Lett.*, 2016, **7**, 1225-1230.
28 D. P. Hoffman, S. R. Ellis and R. A. Mathies, *J. Phys. Chem. A*, 2014, **118**, 4955-4965.
29 S. Sasaki, G. P. C. Drummen and G.-i. Konishi, *J. Mater. Chem. C*, 2016, **4**, 2731-2743.
30 Z. R. Grabowski, K. Rotkiewicz and W. Rettig, *Chem. Rev.*, 2003, **103**, 3899-4032.
31 R. Gepshtein, D. Huppert and N. Agmon, *J. Phys. Chem. B*, 2006, **110**, 4434-4442.
32 R. Hu, E. Lager, A. Aguilar-Aguilar, J. Liu, J. W. Y. Lam, H. H. Y. Sung, I. D. Williams, Y. Zhong, K. S. Wong, E. Peña-Cabrera and B. Z. Tang, *J. Phys. Chem. C*, 2009, **113**, 15845-15853.
33 S. Rafiq, B. K. Rajbongshi, N. N. Nair, P. Sen and G. Ramanathan, *J. Phys. Chem. A*, 2011, **115**, 13733-13742.
34 I. V. Polyakov, B. L. Grigorenko, E. M. Epifanovsky, A. I. Krylov and A. V. Nemukhin, *J. Chem. Theory Comput.*, 2010, **6**, 2377-2387.
35 A. Svendsen, H. V. Kiefer, H. B. Pedersen, A. V. Bochenkova and L. H. Andersen, *J. Am. Chem. Soc.*, 2017, **139**, 8766-8771.
36 B. Dunlap, K. C. Wilson and D. W. McCamant, *J. Phys. Chem. A*, 2013, **117**, 6205-6216.
37 D. P. Hoffman and R. A. Mathies, *Acc. Chem. Res.*, 2016, **49**, 616-625.
38 C. Fang, L. Tang, B. G. Oscar and C. Chen, *J. Phys. Chem. Lett.*, 2018, **9**, 3253–3263.
39 A. F. Bell, X. He, R. M. Wachter and P. J. Tonge, *Biochemistry*, 2000, **39**, 4423-4431.
40 X. He, A. F. Bell and P. J. Tonge, *J. Phys. Chem. B*, 2002, **106**, 6056-6066.
41 W. Liu, Y. Wang, L. Tang, B. G. Oscar, L. Zhu and C. Fang, *Chem. Sci.*, 2016, **7**, 5484-5494.
42 C. Chen, W. Liu, M. S. Baranov, N. S. Baleeva, I. V. Yampolsky, L. Zhu, Y. Wang, A. Shamir, K. M. Solntsev and C. Fang, *J. Phys. Chem. Lett.*, 2017, **8**, 5921–5928.
43 B. G. Levine and T. J. Martínez, *Annu. Rev. Phys. Chem.*, 2007, **58**, 613-634.

44 W. Liu, F. Han, C. Smith and C. Fang, *J. Phys. Chem. B*, 2012, **116**, 10535-10550.
45 D. R. Dietze and R. A. Mathies, *ChemPhysChem*, 2016, **17**, 1224–1251.
46 A. Follenius-Wund, M. Bourotte, M. Schmitt, F. Iyice, H. Lami, J.-J. Bourguignon, J. Haiech and C. Pigault, *Biophys. J.*, 2003, **85**, 1839-1850.
47 P. Altoe, F. Bernardi, M. Garavelli, G. Orlandi and F. Negri, *J. Am. Chem. Soc.*, 2005, **127**, 3952-3963.
48 F. Han, W. Liu and C. Fang, *Chem. Phys.*, 2013, **422**, 204-219.
49 S. P. Laptenok, J. Conyard, P. C. B. Page, Y. Chan, M. You, S. R. Jaffrey and S. R. Meech, *Chem. Sci.*, 2016, **7**, 5747-5752.
50 L. Tang, W. Liu, Y. Wang, Y. Zhao, B. G. Oscar, R. E. Campbell and C. Fang, *Chem. Eur. J.*, 2015, **21**, 6481-6490.
51 S. S. Stavrov, K. M. Solntsev, L. M. Tolbert and D. Huppert, *J. Am. Chem. Soc.*, 2006, **128**, 1540-1546.
52 L. Tang, Y. Wang, L. Zhu, K. Kallio, S. J. Remington and C. Fang, *Phys. Chem. Chem. Phys.*, 2018, **20**, 12517–12526.
53 A. Usman, O. F. Mohammed, E. T. J. Nibbering, J. Dong, K. M. Solntsev and L. M. Tolbert, *J. Am. Chem. Soc.*, 2005, **127**, 11214-11215.
54 C. Chen, L. Zhu and C. Fang, *Chin. J. Chem. Phys.*, 2018, **31**, 492-502.
55 B. G. Oscar, W. Liu, Y. Zhao, L. Tang, Y. Wang, R. E. Campbell and C. Fang, *Proc. Natl. Acad. Sci. U. S. A.*, 2014, **111**, 10191-10196.
56 C. Fang, J. Wang, A. K. Charnley, W. Barber-Armstrong, A. B. Smith, III, S. M. Decatur and R. M. Hochstrasser, *Chem. Phys. Lett.*, 2003, **382**, 586-592.
57 P. J. M. Johnson, A. Halpin, T. Morizumi, V. I. Prokhorenko, O. P. Ernst and R. J. D. Miller, *Nat. Chem.*, 2015, **7**, 980-986.
58 W. Liu, L. Wang, F. Han and C. Fang, *Opt. Lett.*, 2013, **38**, 3304-3307.
59 M. G. Chiariello and N. Rega, *J. Phys. Chem. A*, 2018, **122**, 2884-2893.
60 S. Lochbrunner, A. J. Wurzer and E. Riedle, *J. Chem. Phys.*, 2000, **112**, 10699-10702.
61 N. Huse, B. D. Bruner, M. L. Cowan, J. Dreyer, E. T. J. Nibbering, R. J. D. Miller and T. Elsaesser, *Phys. Rev. Lett.*, 2005, **95**, 147402.
62 M. Liebel, C. Schnedermann, G. Bassolino, G. Taylor, A. Watts and P. Kukura, *Phys. Rev. Lett.*, 2014, **112**, 238301.
63 L. M. Tolbert and K. M. Solntsev, *Acc. Chem. Res.*, 2002, **35**, 19-27.
64 O. F. Mohammed, J. Dreyer, B.-Z. Magnes, E. Pines and E. T. J. Nibbering, *ChemPhysChem*, 2005, **6**, 625-636.
65 G. Granucci, J. T. Hynes, P. Millie and T.-H. Tran-Thi, *J. Am. Chem. Soc.*, 2000, **122**, 12243-12253.
66 D. B. Spry and M. D. Fayer, *J. Chem. Phys.*, 2008, **128**, 084508.
67 A. Petrone, P. Caruso, S. Tenuta and N. Rega, *Phys. Chem. Chem. Phys.*, 2013, **15**, 20536-20544.
68 K. Wynne, G. D. Reid and R. M. Hochstrasser, *J. Chem. Phys.*, 1996, **105**, 2287-2297.
69 L. Wang, G. B. Griffin, A. Zhang, F. Zhai, N. E. Williams, R. F. Jordan and G. S. Engel, *Nat. Chem.*, 2017, **9**, 219-225.
70 T. Kumpulainen, B. Lang, A. Rosspeintner and E. Vauthey, *Chem. Rev.*, 2017, **117**, 10826-10939.
71 J. P. Malhado and J. T. Hynes, *J. Chem. Phys.*, 2012, **137**, 22A543.
72 S. Takeuchi, S. Ruhman, T. Tsuneda, M. Chiba, T. Taketsugu and T. Tahara, *Science*, 2008, **322**, 1073-1077.
73 A. Weigel and N. P. Ernsting, *J. Phys. Chem. B*, 2010, **114**, 7879-7893.
74 C. R. S. Mooney, D. A. Horke, A. S. Chatterley, A. Simperler, H. H. Fielding and J. R. R. Verlet, *Chem. Sci.*, 2013, **4**, 921-927.
75 G.-J. Huang, J.-H. Ho, C. Prabhakar, Y.-H. Liu, S.-M. Peng and J.-S. Yang, *Org. Lett.*, 2012, **14**, 5034-5037.
76 K. Brejc, T. K. Sixma, P. A. Kitts, S. R. Kain, R. Y. Tsien, M. Ormö and S. J. Remington, *Proc. Natl. Acad. Sci. U. S. A.*, 1997, **94**, 2306-2311.
77 J. Y. Hasegawa, K. Fujimoto, B. Swerts, T. Miyahara and H. Nakatsuji, *J. Comput. Chem.*, 2007, **28**, 2443-2452.
78 J. W. Park and Y. M. Rhee, *J. Am. Chem. Soc.*, 2016, **138**, 13619-13629.
79 M. S. Baranov, K. A. Lukyanov, A. O. Borissova, J. Shamir, D. Kosenkov, L. V. Slipchenko, L. M. Tolbert, I. V. Yampolsky and K. M. Solntsev, *J. Am. Chem. Soc.*, 2012, **134**, 6025-6032.
80 C. Chen, M. S. Baranov, L. Zhu, N. S. Baleeva, A. Y. Smirnov, S. Zaitseva, I. V. Yampolsky, K. M. Solntsev and C. Fang, *Chem. Commun.*, 2019, **55**, 2537-2540.
81 A. Baldridge, J. Kowalik and L. M. Tolbert, *Synthesis*, 2010, **2010**, 2424-2436.
82 S. Kojima, H. Ohkawa, T. Hirano, S. Maki, H. Niwa, M. Ohashi, S. Inouye and F. I. Tsuji, *Tetra. Lett.*, 1998, **39**, 5239-5242.
83 X. He, A. F. Bell and P. J. Tonge, *FEBS Lett.*, 2003, **549**, 35-38.
84 J. J. Snellenburg, S. P. Laptenok, R. Seger, K. M. Mullen and I. H. M. van Stokkum, *J. Stat. Softw.*, 2012, **49**, 1-22.
85 L. Zhu, W. Liu and C. Fang, *Appl. Phys. Lett.*, 2014, **105**, 041106.
86 M. J. Frisch, G. W. Trucks, H. B. Schlegel, G. E. Scuseria, M. A. Robb, J. R. Cheeseman, G. Scalmani, V. Barone, B. Mennucci, G. A. Petersson, H. Nakatsuji, M. Caricato, X. Li, H. P. Hratchian, A. F. Izmaylov, J. Bloino, G. Zheng, J. L. Sonnenberg, M. Hada, M. Ehara, K. Toyota, R. Fukuda, J. Hasegawa, M. Ishida, T. Nakajima, Y. Honda, O. Kitao, H. Nakai, T. Vreven, J. J. A. Montgomery, J. E. Peralta, F. Ogliaro, M. Bearpark, J. J. Heyd, E. Brothers, K. N. Kudin, V. N. Staroverov, R. Kobayashi, J. Normand, K. Raghavachari, A. Rendell, J. C. Burant, S. S. Iyengar, J. Tomasi, M. Cossi, N. Rega, J. M. Millam, M. Klene, J. E. Knox, J. B. Cross, V. Bakken, C. Adamo, J. Jaramillo, R. Gomperts, R. E. Stratmann, O. Yazyev, A. J. Austin, R. Cammi, C. Pomelli, J. W. Ochterski, R. L. Martin, K. Morokuma, V. G. Zakrzewski, G. A. Voth, P. Salvador, J. J. Dannenberg, S. Dapprich, A. D. Daniels, Ö. Farkas, J. B. Foresman, J. V. Ortiz, J. Cioslowski and D. J. Fox, *Gaussian 09, Revision B.1*, Gaussian, Inc., Wallingford, CT, 2009.
87 O. V. Gritsenko, P. R. T. Schipper and E. J. Baerends, *J. Chem. Phys.*, 1997, **107**, 5007-5015.
88 S.-J. Baek, A. Park, Y.-J. Ahn and J. Choo, *Analyst*, 2015, **140**, 250-257.

Textual abstract (20 words) for the contents pages

Upon photoexcitation, a delayed structural bending motion facilitates the “dark” GFP-chromophore ring-twisting isomerization in reaching a conical intersection in solution.

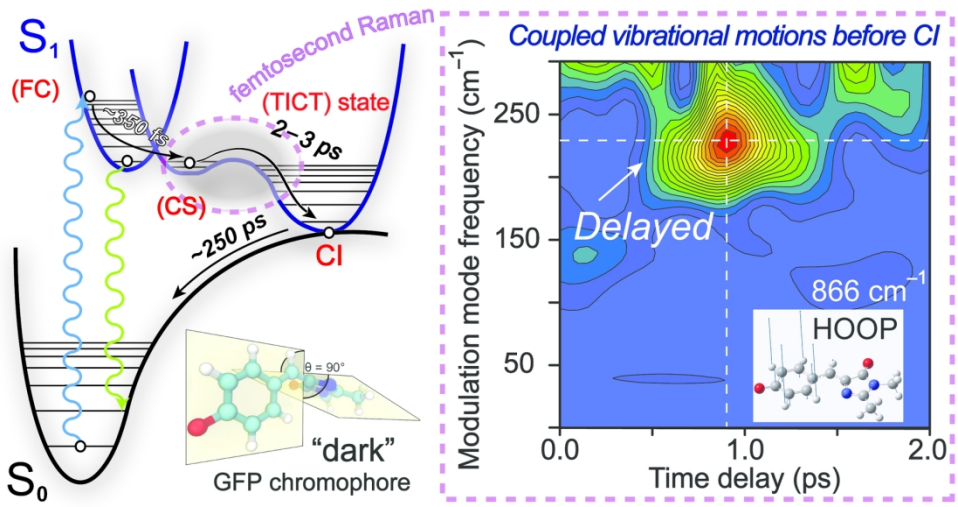

80x40mm (600 x 600 DPI)